Dynamic Frequency Tracking for Voltage and Frequency Regulation of Wind Driven Doubly Fed Induction Generator in Standalone mode

S. R. Mohanrajan ‡, A. Vijayakumari and K. Kottayil Sasi

Department of Electrical and Electronics Engineering, Amrita School of Engineering, Coimbatore,

Amrita Vishwa Vidyapeetham, India

(sr_mohanrajan@cb.amrita.edu, a_vijayakumari@cb.amrita.edu, kk_sasi@cb.amrita.edu)

‡Corresponding Author: Mohanrajan S R, Department of Electrical and Electronics Engineering,

Amrita School of Engineering, Coimbatore, Amrita Vishwa Vidyapeetham, India: Tel: +91 9842825931,

sr_mohanrajan@cb.amrita.edu

Received: 24.09.2020 Accepted:16.10.2020

Abstract- This paper presents a simple and effective method for dynamic regulation of stator frequency and voltage in wind-driven doubly fed induction generator (DFIG) for standalone operation. The proposed Dynamic Frequency Tracker (DFT) is a combination of feed forward–feedback control loops to maintain stator frequency and voltage at the rated values when the load, or the wind power, or both vary independently. The measured rotor speed is used in the feedforward loop to obtain the reference rotor frequency, whereas the rotor reference voltage is obtained from the feedback loop. The magnetic stability of the DFIG is ensured by keeping the voltage-to-frequency ratio constant in the inverter reference voltage calculations. Validation of the proposed DFT has been carried out through laboratory tests involving hardware units of wind turbine emulator and DFIG. Tests are conducted under steady state and transient state conditions, separately for super synchronous and sub synchronous modes of the generator, wherein wind speed and load on the stator are varied too. Stator loads of unity and lagging power factors have been considered. Results of all the tests confirmed stable and satisfactory regulation of the stator voltage and frequency.

Keywords voltage and frequency regulation, doubly fed induction generator, dynamic frequency tracking, sub synchronous, super synchronous.

1. Introduction

Isolated micro grid is a recent concept promoted in developing economies to tackle supply-demand gap that also allows higher renewable energy penetration into their electric utilities [1,2]. Absence of electric power grid is very common in rural and outlying areas in developing and under-developed countries due to economical and geographical constraints [3-6]. Usually those places are either unelectrified or powered using diesel-electric generators to feed mostly domestic lighting and irrigation pumps. For such cases, solar and wind electric systems are viable options with short payback periods, as there is no recurring fuel cost as in the case of diesel generator [7,8]. Standalone solar PV systems have become ubiquitous owing to availability of matured technology and grid parity [9-11], whereas wind turbines are yet to establish in off-grid generation on a commercial scale due to the open ended research and development issues such as voltage and frequency regulation, variable speed operation, active and reactive power control, maximum power tracking, energy storage management, etc. Possible simultaneous variations in both the load and the wind speed demand a complex power balance control to arbitrate the power mismatch when not connected to the legacy grid [12]. However, the variable speed wind turbine generators (WTG) have an edge over the fixed speed WTG in this regard [13-15].

Different types of variable speed WTGs with simple to complex controls have been tried in stand-alone mode to achieve optimum utilization of wind energy, simultaneously targeting better power quality and balance with and without

energy storage [13,16-19]. Permanent magnet generator had been the natural choice for variable speed operation of stand-alone wind systems [20] as it does not require an external source of magnetisation; yet the full rated inverter and the battery management circuits make it complex and costly. Recently, Doubly Fed Induction Generator (DFIG) has gained visibility in standalone wind applications [21-24] due to their unique capability to maintain the stator voltage and frequency at any desired level besides managing energy storage, all with a single fractional sized inverter.

Direct voltage control and stator flux oriented control have been suggested for stator voltage and frequency regulation in standalone DFIGs [25]; but, these demand intense trigonometric computations in dq/αβ co-ordinate transformations of the sensed three phase stator voltages and rotor currents. The complex computations involved there demand high end digital controllers with their undue delays resulting in sluggish system response against change in wind or load and exhibiting poor transient performance [26-31]. In contrast, simpler methods using sensor-less speed control have also been developed [32-34], accounting the wind speed variations through deviations in stator voltage and frequency; the main challenge reported in such controllers is the large time delay involved in computing the frequency during the wind speed variation. This computational delay will give rise to longer system response time eventually yielding poor stator voltage or frequency regulation especially during wind speed and/or load variations. Such fluctuations in standalone systems may create catastrophic effects leading to total system failure due to power mismatch and system instability.

The authors have proposed in this paper stand-alone operation of DFIG with dynamic frequency tracking control which utilizes sensed rotor speed information to compute the reference frequency for use in the control loops. The proposed controller uses a feedforward – feedback combinational scheme that helps reduction in the frequency computation time with two sensors, one each for measuring the speed and the stator voltage, in contrast to six sensors in previously suggested methods [25,31,35-37]. Besides reducing the computation time, it also reduces the number of sensed signals in comparison with the research in the past.

2. Control Strategy for Stator Regulation in Standalone DFIG

The concept of dynamic frequency tracking control for stator voltage and frequency regulation is conceived from the stator voltage equation of a standalone DFIG. The steady state equivalent circuit of DFIG operating in stand-alone mode [25] is given in Fig.1. in which V_r represents the per phase rotor injected voltage, E is the air-gap voltage, a is stator to rotor turns ratio, I_s is per phase stator current, I_r is the rotor current referred to stator, V_s is the generated stator terminal voltage, R_r is the rotor resistance referred to stator, X_r is the rotor reactance referred to stator, R_s and X_s are stator resistance and reactance respectively, R_m and X_m are stator core loss resistance and magnetising reactance respectively, s is the slip and $R+jX$ represents the load impedance on the stator.

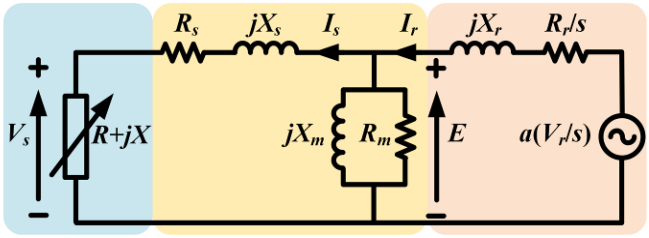

Fig.1. Steady state equivalent circuit per phase of standalone DFIG

By applying Kirchoff's Voltage Law in the two loops,

$$a\frac{V_r}{s} = E + I_r\left(\frac{R_r}{s} + jX_r\right) \tag{1}$$

$$E = V_s + \frac{V_s}{(R+jX)}(R_s + jX_s) \tag{2}$$

Then by applying Kirchoff's Current Law at the node,

$$I_r = \frac{V_s}{R+jX} + V_s\left(1+\frac{R_s+jX_s}{R+jX}\right)\left(\frac{1}{R_m}+\frac{1}{jX_m}\right) \tag{3}$$

On substituting E and I_r in equation (1), the rotor voltage referred to stator can be expressed as,

$$2a\frac{V_r}{s} = V_s + \frac{V_s}{(R+jX)}(R_s+jX_s) + \frac{V_s}{R+jX} + V_s\left(1+\frac{R_s+jX_s}{R+jX}\right)\left(\frac{1}{R_m}+\frac{1}{jX_m}\right)\left(\frac{R_r}{s}+jX_r\right) \tag{4}$$

Rearranging equation (4), the stator voltage can be obtained as,

$$V_s = \frac{\left(a\frac{V_r}{s}\right)}{\left(1+\frac{1+(R_s+jX_s)}{(R+jX)}+\left(1+\frac{R_s+jX_s}{R+jX}\right)\left(\frac{1}{R_m}+\frac{1}{jX_m}\right)\left(\frac{R_r}{s}+jX_r\right)\right)} \tag{5}$$

Equation (5) helps to infer that the stator voltage of DFIG in the stand-alone mode is influenced by the three factors viz. the wind speed, the injected rotor voltage, and the load impedance on the stator.

An increase in the load on the stator, while working in steady state with a constant wind speed, will cause an increase in the slip and in turn a reduction in the stator voltage. The stator voltage can then be restored by an appropriate increase in the injected rotor voltage and power, thus balancing the increased load demand. On the other hand, an increase in the wind speed while working in steady state will cause a decrease in slip, giving rise to an increase in stator voltage. Then the stator voltage can be restored by an appropriate reduction in the rotor injected voltage and power in order to maintain the stator voltage at its rated value as well as the power balance. In both cases, the change in rotor speed will alter the respective wind power input owing to the dependence of wind turbine power (WT) coefficient, Cp, on

its shaft speed, Ω_r, as is evident from the equations (6), (7) and (8).

$$P_{WT} = \frac{\pi}{2}\rho R^2 V_w^3 C_p \quad (6)$$

$$C_P = f(\lambda, \beta) \quad (7)$$

$$\lambda = \frac{\Omega_r R}{V_w} \quad (8)$$

where, P_{WT} is the wind turbine power output in Watt, ρ is air density in kg/m3, R is turbine sweep radius in m, V_w is wind speed in m/s, λ is tip speed ratio of the turbine, and, β is its blade pitch angle. Such Cp variation can be either an increase or a decrease in its value. However, this power variation too can be addressed in the rotor power injection – if the turbine power is in excess of the load demand on DFIG stator, it can be fed back to the rotor; if there is a deficit, required additional power can be availed from a battery storage and injected through the rotor.

Thus, the methodology of voltage regulation in the standalone mode of DFIG should target balancing equation (5) for a desired stator voltage, $V_{s(ref)}$, irrespective of change either in load, or in wind speed, or in both. This can be realised by the magnitude control of the rotor injected voltage through the rotor side converter while simultaneously maintaining the air gap flux at its rated value.

Further, the stator frequency also varies when there is imbalance between the wind power input and the power delivered to the load; this causes the magnetic field of the machine to rotate at a speed other than the synchronous speed. Therefore, the magnetic field in the stand-alone DFIG needs to be established by the rotor side quantities; the magnetic field rotating at synchronous speed can ensure the rated frequency in the stator, $\omega_{s(ref)}$. The frequency of the air gap flux will be jointly decided by the slip and the injected rotor frequency.

Assuming (1:1) gear ratio between the turbine and the generator, Ω_r is the mechanical angular speed of the DFIG rotor in rad/s. If ω_r and ω_s are the rotor circuit frequency and the rated stator circuit frequency respectively in rad/s, then equation (9) relates the two where P is the number of poles,

$$\omega_r = \omega_s - \Omega_r \frac{P}{2} \quad (9)$$

So, when Ωr varies upon a wind speed/load variation, ω_r can be varied such that the air gap flux can be retained at the rated synchronous speed. ω_r above ω_s indicates operation in super-synchronous mode and the opposite condition indicates sub-synchronous mode. However, varying the rotor frequency independently will cause air gap flux variation leading to magnetic instability and a consequent voltage variation. Instead, the magnitude of the injected rotor voltage is to be maintained at the rated V/f ratio of the machine for every rotor frequency. Providing the voltage, $V_{r(ref)}$ and frequency, $\omega_{r(ref)}$ values thus obtained as the references for the rotor side inverter will ensure stator side voltage and frequency regulation. Such a scheme is devised here and named as *dynamic frequency tracking* which is presented in the next section.

3. Dynamic Frequency Tracking

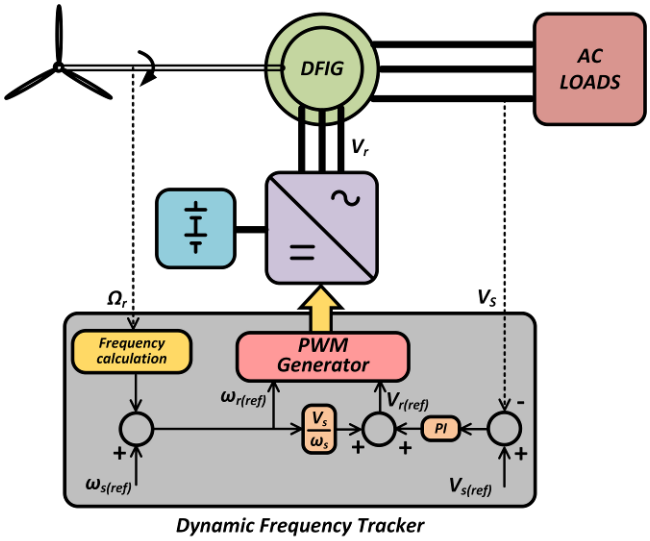

Fig. 2. Standalone DFIG enabled with Dynamic Frequency Tracking

The stand-alone DFIG system involving dynamic frequency tracking is shown in Fig.2, in which the power plant is feeding a three phase balanced AC load. A source/sink of power (in the form of a battery) is provided in the rotor circuit, so that a bi-directional power flow between the stator and the rotor of the DFIG could be achieved. The function of the dynamic frequency tracker (DFT) is to obtain the reference magnitude and frequency for the rotor injection through the rotor side converter to regulate the stator quantities for any combination of wind speed and load. The rotor side converter will be made to work as an inverter when DFIG is working in sub-synchronous mode, demanding a power injection into the rotor; while it works in rectifier mode when DFIG is working in super-synchronous mode, demanding evacuation of power outwards from the rotor. The proposed DFT uses a feed-forward plus feedback control for accomplishing better dynamic response to accurately follow the slip variations, as shown in the figure. The feed-forward loop consists of the digital speed sensor for rotor speed measurement, while the voltage feedback loop is employed to track the set point stator voltage and mitigate its deviation from its nominal value. Feed-forward loop is designed with direct computation of ωr from the speed encoder output through microcontroller to improve the transient response by making it instantaneous. Accordingly, the corrective action is taken jointly by the two control loops against the disturbances triggered by the load/wind speed changes.

The rotor voltage reference when calculated from the constant V/f ratio can regulate the stator voltage under no-load condition. But once the DFIG is loaded, the stator terminal voltage falls due to the internal voltage drops in proportion to the current delivered by the machine. Hence a PI compensator is included in the voltage loop to track the stator voltage change under loaded condition. Further, the

output of the PI compensator is added with the rotor voltage calculated from the fixed *V/f* ratio to obtain the final rotor reference voltage. The rotor injection frequency and voltage serve as the references for the PWM block to generate pulses for the rotor side inverter to physically generate the computed rotor reference voltage.

4. Laboratory Emulation of standalone DFIG

Validation of the proposed DFT in hardware demands an experimental setup in the laboratory. The block diagram of the experimental setup is presented in Fig.3. It represents a WT driven DFIG in standalone mode.

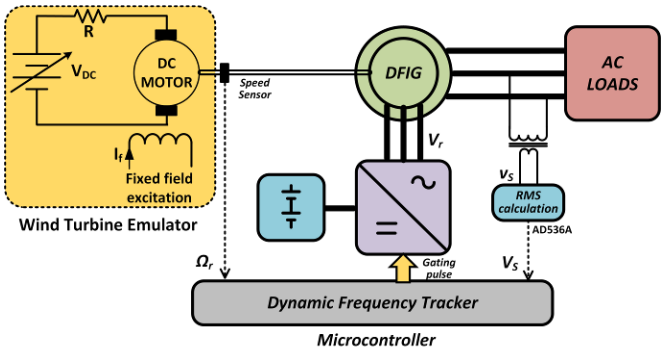

Fig.3. Hardware implementation scheme of the stand-alone DFIG with DFT

The test system has two sections – a WT emulator on the left and the DFT on the right. WT emulation is indispensable in the testing of wind driven DFIG, as otherwise the prime mover of the generator may not exhibit WT characteristics. The generic characteristics of a WT correlate the wind speed with the shaft speed and WT power output. Laboratory testing of DFIG for assessment of the impact of varying wind or changing load therefore demands a WT emulator. The WT is emulated in this work using a DC motor which acts as the prime mover for the DFIG. A simple WT emulation method suggested by Fernando et. al. [38,39] with the separately excited DC motor connected in series with a resistor in its armature circuit is used here. The mechanical power output of the motor is expressed as,

$$P_m = \frac{kI_f}{R+R_a}\left(V_{DC}\omega - kI_f\omega^2\right) \tag{10}$$

where, ω is the speed dc motor in rad/s, k is the back EMF constant, I_f is the field current, V_{DC} is the DC input voltage to the emulator, R is the resistance connected in series with the armature and R_a is the armature resistance. P_m of equation (10) represents P_{WT} of equation (6). The series resistor R is such chosen that the WT emulator exhibits the Cp-λ characteristics of the desired WT design. The chosen specifications of the WT, the DC motor and the slip ring induction machine (SRIM) used as the DFIG are as given in Table1.

Table1: Ratings of DC motor, SRIM and the emulated WT

WT	Rating	DC Motor	Rating	SRIM	Rating
Power	500W	Power	1.1kW	Power	1.1kW
Rotor Diameter	0.75m	Armature Voltage	230 V	Voltage	415V
$C_p$max	0.4	Armature Current	4.7 A	Stator Current	4 A
$\lambda_{optimal}$	6.25	Field current	0.8 A	Rotor Current	20 A
Rated wind speed	10	Speed	1500 rpm	Speed	980 rpm

The Cp-λ characteristic equation adopted from MATLAB/Simulink library [40] is,

$$C_P(\lambda,\beta) = c_1\left(\frac{c_2}{\lambda_i} - c_3\beta - c_4\right)e^{-\left(\frac{c_5}{\lambda_i}\right)} + c_6\lambda \tag{11}$$

$$\frac{1}{\lambda_i} = \frac{1}{\lambda + 0.08\beta} - \frac{0.035}{\beta^3+1} \tag{12}$$

where, c1 to c6 are the coefficients with values assigned [40] as, c_1=0.5176, c_2=116, c_3=0.4, c_4=5, c_5=21 and c_6=0.0068. The WT pitch angle variation is assumed to be zero being a fixed pitch turbine.

The DFT control is implemented in the microcontroller with computation of RMS values of the electrical parameters in the commercial IC AD536A. The rotor side converter is a Semikron made three phase IGBT bridge rated at 600 V, 30A. An optical speed encoder is used to sense the shaft speed in the experimental setup. The experimental setup is shown in Fig. 4.

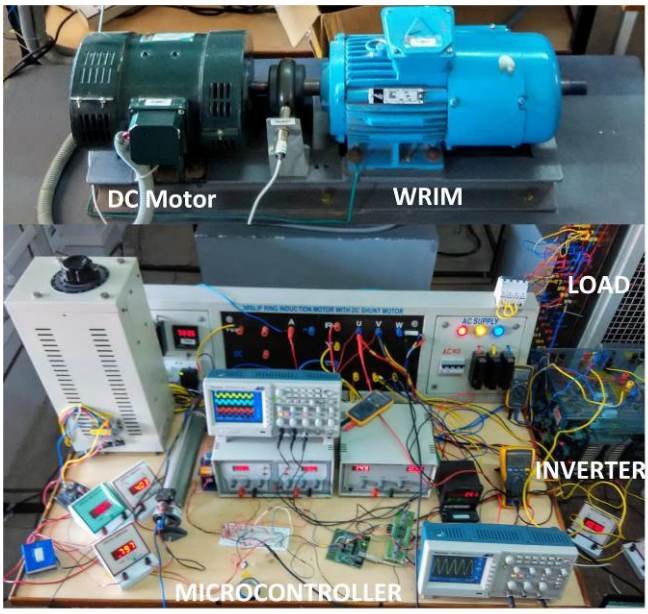

Fig. 4. Experimental setup of standalone DFIG

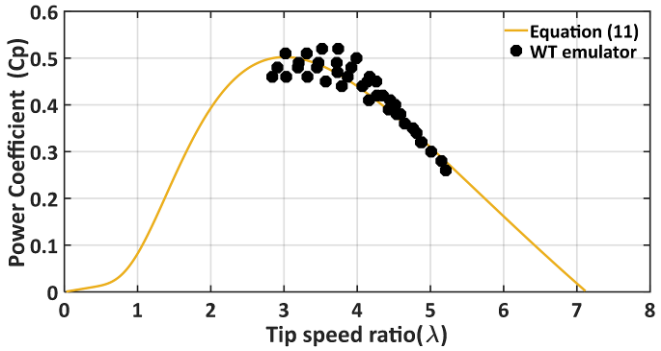

Fig. 5. Cp-λ curve of the WT emulator

The 500 W wind turbine was emulated for testing the DFIG with the proposed DFT in a range of wind speed from 6 to 10 m/s. The WT emulator was first tested and validated by comparing its *Cp*-λ plot with that of equation (11) and mapping the wind speeds against the DC armature voltages. The *Cp*-λ characteristic curve of the emulated WT is plotted using equation (11) in Fig. 5 on which superimposed are the tested points of operation of the actual WT emulator developed in the lab. It can be observed in Fig. 5 that the *Cp*-λ characteristics of the emulated WT closely follows equation (11) for the range of λ from 3 to 5 and that forms the window in which the testing of the WT driven DFIG is carried out. Equating Pm to PWT and then computing v by use of equation (6), the DC input voltage is mapped to the wind speed. These results are given in Table 2.

Table 2. Test results of the WT emulator

V_{DC} (V)	P_{WT} (W)	v (m/s)
265	417	10
249	367	9.5
233	324	9
217	264	8.5
202	211	8
187	162	7.5
172	112	7
158	63	6.5

5. Validation of DFT in standalone DFIG

The proposed DFT is tested in both steady state and transient operating conditions of the standalone DFIG system, as well as in both sub-synchronous and super synchronous generation modes. The tests are carried out for a range of operating conditions formulated by appropriate combinations of the load and the available wind speed. The steady state test conditions considered are (i) Super-synchronous generation, and (ii) Sub-synchronous generation. Similarly, three transient state test conditions are considered which are (i) step change in wind speed and load under super-synchronous mode, (ii) step change in wind speed and load under sub-synchronous mode, and, (iii) generation mode change (between sub-synchronous and super-synchronous modes) due to change in wind speed and load.

5.1 Steady state performance

i.Super synchronous generation mode

This mode of generation is characterized by a shaft speed above the synchronous speed with the DFIG giving power outputs from both the stator and rotor. That means, the load demand on the DFIG is less than the power generated by the WT and the surplus power is delivered to the rotor side energy storage by the converter.

Test conditions of super synchronous generation established are the following:

(i) a constant wind speed of 10 m/s with which the WT delivers a constant shaft power of 205 W, and,

(ii) a constant wind speed of 9 m/s with which the WT delivers a constant shaft power of 173 W.

Both had 25 % load on the stator represented by a resistive load of 120 W. Both these conditions elicited shaft speeds of 1240 rpm and 1066 rpm respectively, which are above the synchronous speed warranting the super synchronous operation.

The stator and rotor quantities observed in DSO are presented in Fig. 6 and 7 for steady state operation. Three phase voltages and line current in the rotor for the wind speed of 10 m/s are shown in Fig. 6.a. & b; these quantities for the wind speed of 9 m/s are shown in Fig 7.c. & d. Channel 1 and 2 provide the line voltages, and the math operation of DSO is used to obtain the phase voltage which is seen in the third row ($3V_a=V_{ab}+V_{ac}$). Channel 3 is the rotor injected current. The stator voltage is observed to be at 200V RMS with a very strict regulation of ±0.1 % while the frequency is maintained within a narrow band of 48.95Hz to 49.98Hz. The rotor injection frequency established through DFT has been observed as 13.09 Hz at the higher shaft speed of 1240 rpm and as 4.55 Hz at the lower shaft speed of 1066 rpm – both comply with Equation (9).

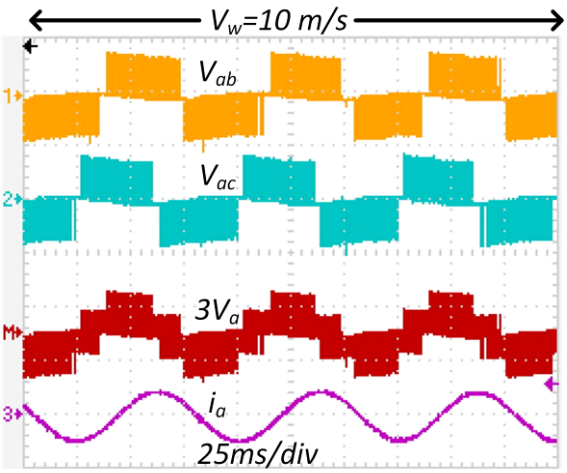

(a)

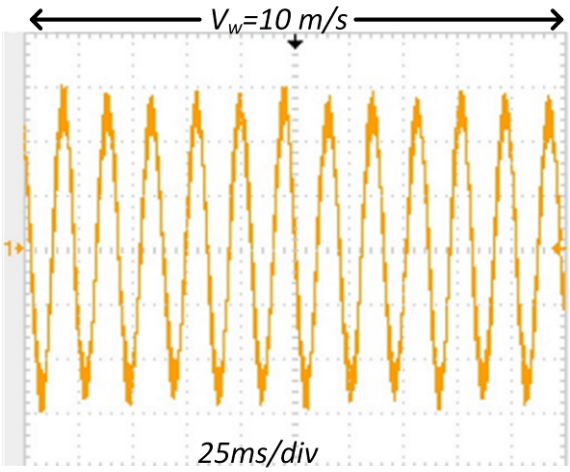

(b)

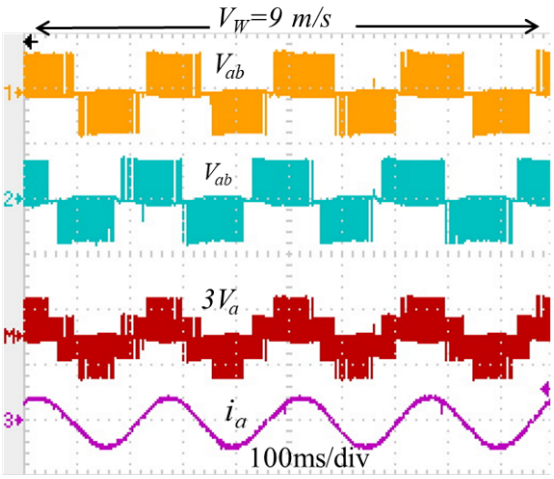

(c)

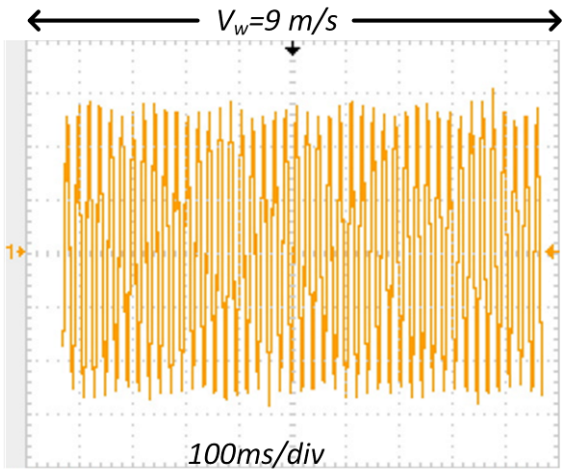

(d)

Fig.6. Steady state super synchronous mode of operation (a) & (c) Rotor side: 3 phase voltages and one line current Y-Scale: Channel 1 & 2 :50V/div, Math:100V/div, Channel 3: 20A/div, (b) & (d) Stator voltage Y- Scale: 108.78 V/div.

ii.Sub-synchronous generation mode

This mode is characterized by a rotor speed less than the synchronous speed, with the load demand on the generator more than the power generated from the wind. The deficit power will be contributed from the rotor side energy storage. The chosen test conditions of sub synchronous generation are the following:

(i) a constant wind speed of 8 m/s with which the WT delivers a constant shaft power of 143 W, and,

(ii) a constant wind speed of 7 m/s with which the WT delivers a constant shaft power of 112 W. With the same load of 120 W, the DFIG operated in sub synchronous at shaft speeds of 885.6 rpm and 711.1 rpm respectively at wind speeds of 8 m/s and 7 m/s. As in super synchronous mode, lower frequency of 4.556 Hz was injected in the rotor with the lower shaft speed and a higher injection frequency of 13.39 Hz at higher speed. Various rotor and stator quantities of the two cases are measured and presented in Fig. 7. Three phase voltages and line current for the wind speed of 8 m/s are shown in Fig 7.a. & b; these quantities for the wind speed of 7 m/s are shown in Fig 7.c. & d. The desired stator voltage and frequency have been achieved in both the cases.

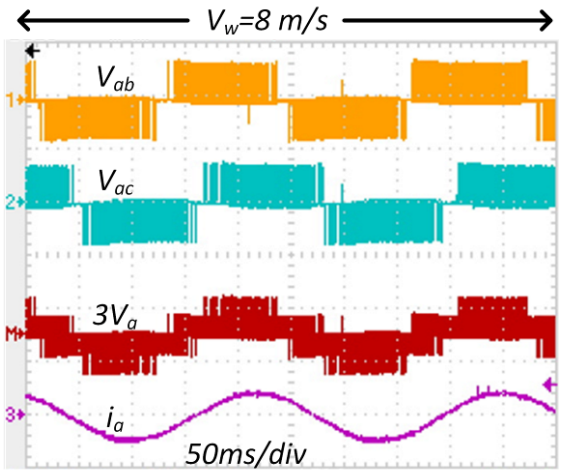

(a)

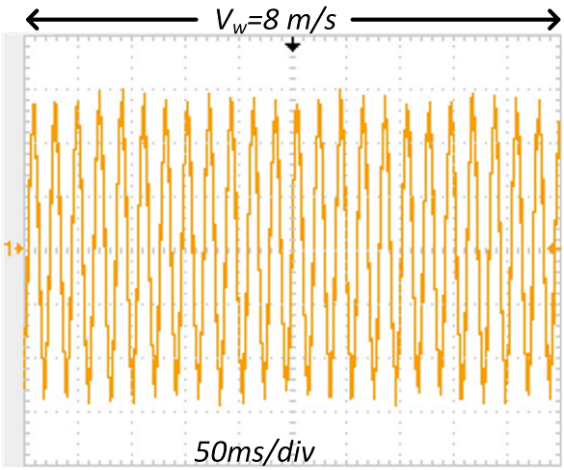

(b)

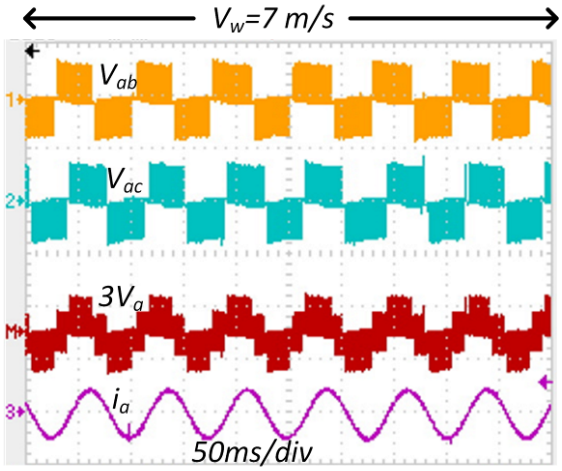

(c)

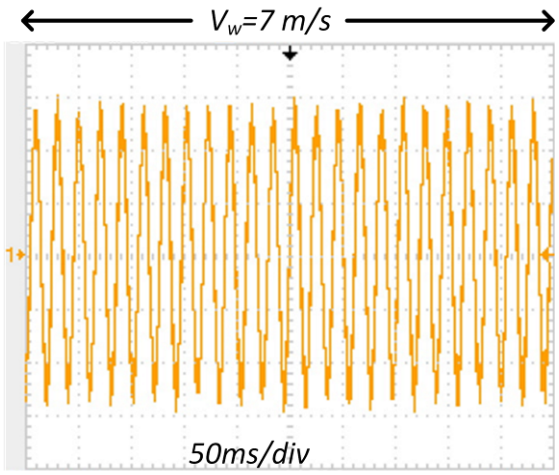

(d)

Fig.7. Steady state sub synchronous mode of operation (a) & (c) Rotor side: 3 phase voltages and one line current Y-Scale: Channel 1 & 2 :50V/div, Math:100V/div, Channel 3: 20A/div, (b) & (d) Stator voltage Y- Scale: 108.78 V/div.

5.2 Transient state performance

Transient state is accomplished in the system by introducing a step change either in the wind speed or in the load. Initially, the experiments are conducted by introducing a transient change in power by careful choice of load as well as the wind speeds, so that the operation will be within the sub synchronous or super synchronous mode. Later, the transient change is introduced such that the operation migrates from super synchronous mode to sub synchronous one, separately for resistive (*R*) and inductive (*RL*) loads.

(i) Transients due to load/wind change in super synchronous mode

With a three-phase 120W resistive load on DFIG stator, the WT emulator is made to ramp down from a wind speed of 10 m/s to 9 m/s, deliberately chosen to confine the operation within super synchronous mode. The shaft powers delivered by the WT are 205 W and 173 W before and after the wind speed change respectively. A shaft speed of 1240 rpm is observed until the wind speed is made to fall, after which the shaft speed changed to 1066 rpm. The waveforms of both stator and rotor quantities are presented in Fig. 8. a & c. Correspondingly a change in the injected frequency from 13.09 Hz to 4.546Hz is observed upon the wind speed change.

The transient state testing has been carried out with an RL load of 100 W, 0.28 power factor lagging maintained on the stator while the wind speed is made to ramp down from 10 m/s to 9 m/s. The observed shaft speed variation from 1245 rpm to 1051 rpm ascertains that the transient event remains within the super synchronous mode, while the rotor injection frequency varied from 13.44 Hz to 3.817 Hz. This transient event is depicted in Fig. 8. b. & d.

In all the four cases, the stator regulation is maintained well within the limits before, after and during all these transient events. Further, the response time in all these transient events

has been observed to be < 50 ms demonstrating the effectiveness of the dynamic frequency tracker.

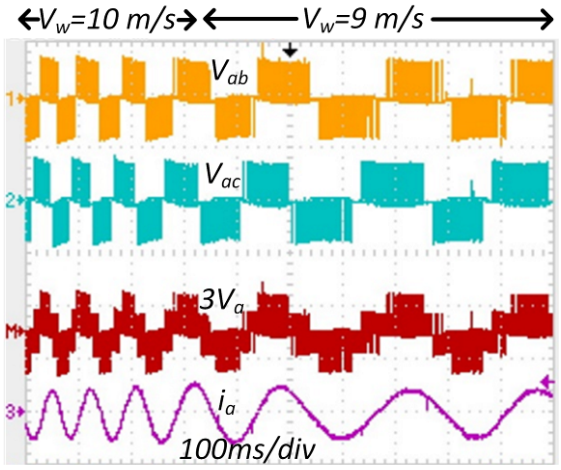

(a)

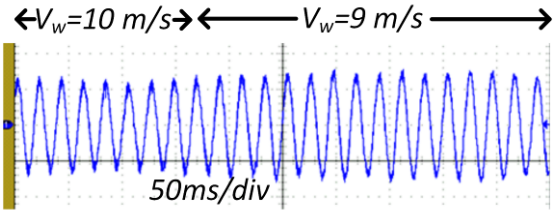

(b)

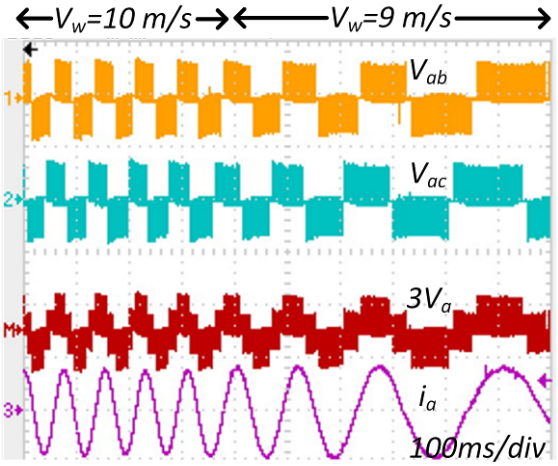

(c)

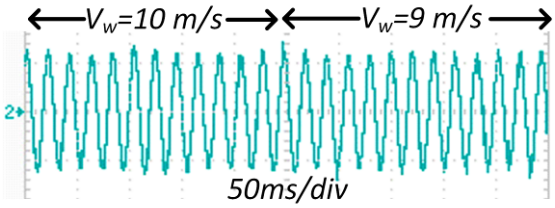

(d)

Fig.8. Transient response within super synchronous mode of operation (a) & (c) Rotor side: 3 phase voltages and one line current Y-Scale: Channel 1 & 2 :50V/div, Math:100V/div, Channel 3: 20A/div, (b) Stator voltage Y- Scale: 217.572 V/div & (d) Stator current Y- Scale: 1.2 A/div.

(ii) Transients due to load/wind change in sub synchronous mode

A transient event has been created in sub-synchronous mode by a step change in the resistive load on stator from 490 W to 240 W while keeping the wind speed constant at 10 m/s. It resulted in a shaft speed variation from 724 rpm to 780 rpm. The stator voltage is regulated by DFT with the rotor injections of 12.35Hz and 9.88Hz respectively for the low and the high shaft speeds. The corresponding changes in rotor and stator circuits are presented in Fig.9.a & b.

The test is repeated by creating another transient event through a load change from 355 W to 105 W while maintaining a constant wind speed of 9m/s. The shaft speed before and after the load change has been observed to be 733 rpm and 794 rpm respectively with a corresponding rotor injection change from 12.11 Hz to 9.13 Hz which was warranted for the stator regulation. The waveforms shown in Fig.9.c. & d reflect impacts of this event.

A third transient event is created with a ramping down in wind speed from 8 m/s to 7 m/s while the stator is delivering a steady RL load of 100W at 0.28 power factor. The shaft speed and rotor injection frequency were found to change from 893 rpm and 4.1 Hz to 714 rpm and 13.11 Hz respectively during this transient event, while maintaining a stable stator voltage and frequency along with a constant load current, as seen in Fig 9.e. & f.

In all the three cases, the stator regulation is well within the limit of ±0.1 %. Additionally, the transition time is observed to be < 50 ms in all the three.

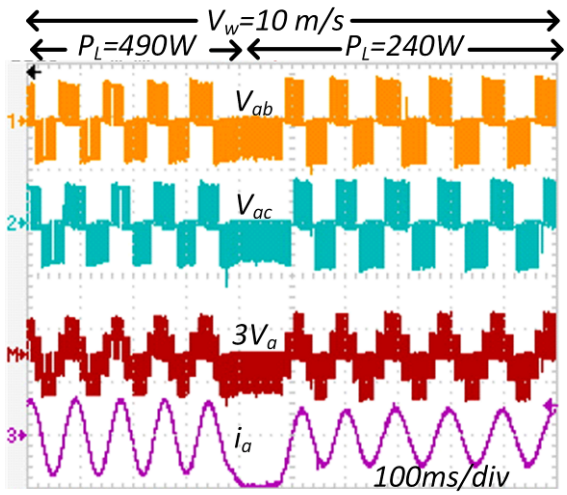

(a)

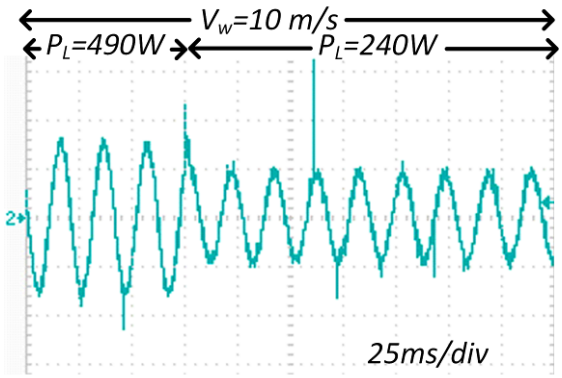

(b)

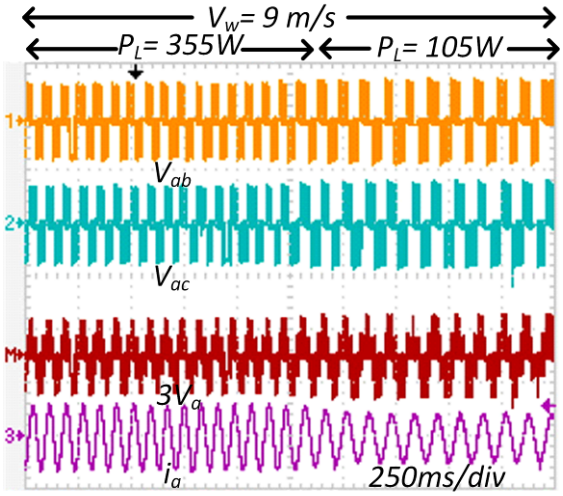

(c)

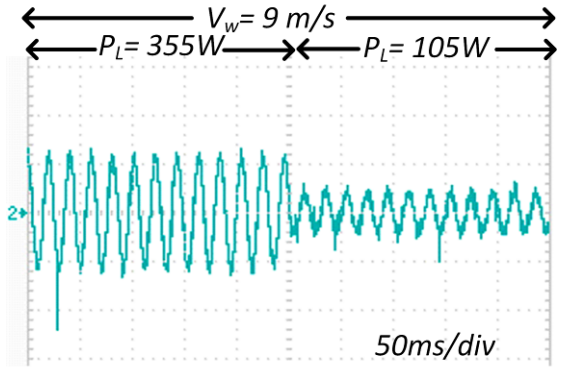

(d)

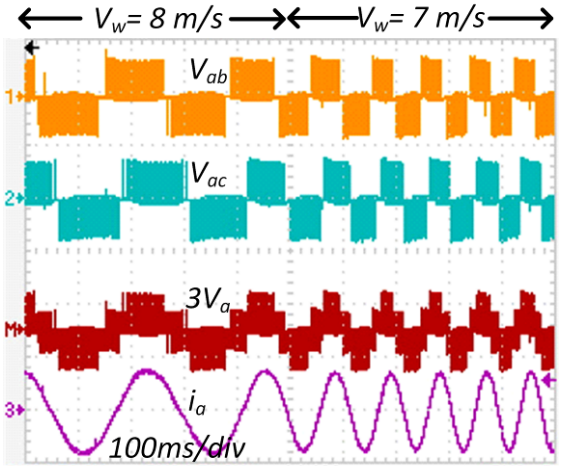

(e)

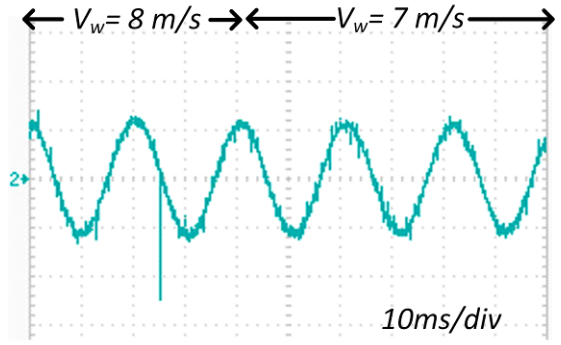

(f)

Fig.9. Transient responses with in sub synchronous mode of operation (a), (c) & (e) Rotor side: 3 phase voltages and one line current Y-Scale: Channel 1 & 2 :50V/div, Math:100V/div, Channel 3: 20A/div, (b), (d) &(f) Stator current Y- Scale: 1.2A/div.

(iii) Transients due to inter mode transition

This transient event is created such that the DFIG is made to migrate from super synchronous mode to sub synchronous one following a fall in wind speed. The machine is feeding a constant load of 100W at 0.28 power factor lagging with a shaft power of 162 W delivered at a wind speed of 9m/s. The WT emulator is then made to reduce the wind speed to 8m/s. The shaft speed is observed to subsequently fall from 1051 rpm to 893 rpm, thus triggering the rotor side converter to deliver power into the rotor in inverter mode. The mode change is evident from the reversal in the phase relationship between the voltages Vab and Vac in Fig. 10.a during the event; Vac leads Vab in the super synchronous mode while Vab leads Vac in the sub synchronous mode. With the rotor current maintaining the same phase relation, a phase reversal of the rotor voltage indicates a power flow reversal in the rotor circuit. The rotor injection frequency is observed as 4.098 Hz in the super synchronous mode and it became 3.817Hz after moving to the sub synchronous mode in order to stabilize the stator voltage at its rated voltage and frequency. The stator and rotor side voltages and currents of this transient event are presented in Fig. 10.a, b & c.

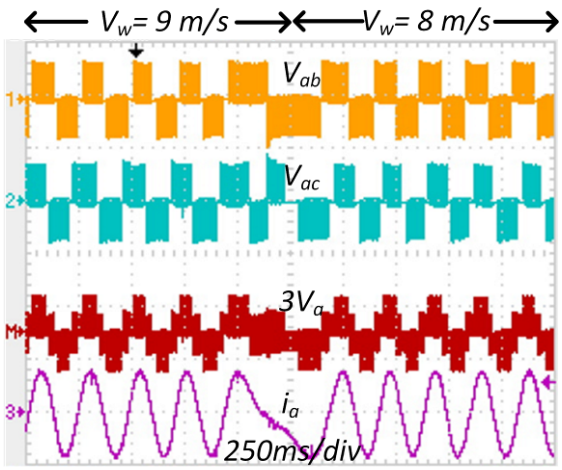

(a)

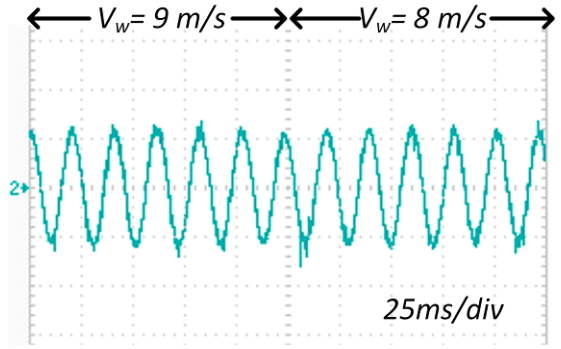

(b)

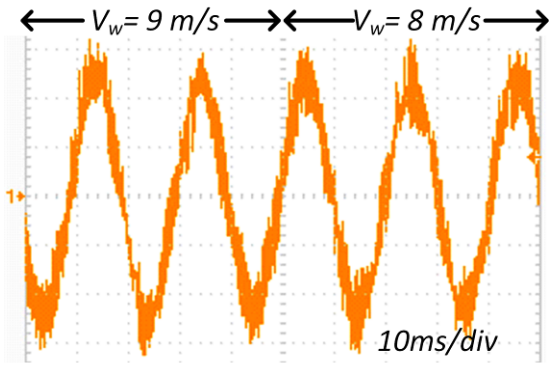

(c)

Fig.10. Transient response of migrating from super synchronous to sub synchronous mode of operation (a) Rotor side: 3 phase voltages and one line current Y-Scale: Channel 1 & 2 :50V/div, Math:100V/div, Channel 3: 20A/div, (b) Stator Current Y- Scale: 1.2 A/div & (d) Stator voltage Y-Scale: 217.572 V/div.

The summary of the test results is presented in Table 3.a. and 3.b for steady state and transient state, respectively. Table 3.c presents the results of similar research in the past available in the literature. The values of voltage and frequency regulations in Table 3.a are found to be highly satisfactory under all load conditions. Comparable values in the past research are not found in the available literature. The intra mode transition time obtained in the present research is in the range of 1 ms to 10 ms which is in dire contrast with 30 ms to 60 ms range seen in the published literature. The comparison in inter mode transition is between (1 ms to 20 ms) obtained in the present work with (50 ms to 60 ms) as reported by past researchers. It substantiates the significant contribution of DFT towards the voltage and frequency regulation in standalone DFIG.

Table :3a Steady state performance metrics of standalone DFIG

Rated stator voltage, Vs=200V, Rated power, P=500W, Rated Stator Frequency, fs =50Hz, Rated Rotor Speed Nr = 800rpm

S.No	V_w (m/s)	Stator load (%)	V_s (V)	f_s (Hz)	Voltage regulation (%)	Frequency Regulation (%)
1	10	70	201	49.99	-0.5	0.02
2	9.5	56	201	49.94	-0.5	0.12
3	9	49	200	49.89	0	0.22
4	8.5	36	200	49.85	0	0.3
5	8	32	200	49.82	0	0.36
6	7.5	26	199	49.8	0.5	0.4

Table : 3b Transient performance metrics of standalone DFIG

Mode Change		V_w (m/s)		% Load		Nr (rpm)		Mode transition Time (ms)
From	To	From	To	From	To	From	To	
Super	Super	10	9	24	24	1240	1066	1★
Sub	Sub	8	7	24	24	885	711	1★
Sub	Sub	10	10	98	48	724	780	5★
Sub	Sub	9	9	71	21	733	794	10★
Sub	Sub	8	7	20	20	893	714.5	0.5 ★★
Super	Sub	9	8	24	24	1066	885	20★
Super	Sub	9	8	20	20	1051	893	1 ★★

★ R Load, ★★ RL Load

Table: 3c Transient performance metrics published in literature

Mode Change		Load		Transition Time (ms)
From	To	From	To	
sub	sub	0	1kW	30 [28]
sub	sub	1kW	2kW	30 [28]
sub	sub	2kW	1kW	40 [28]
Sub	super	2kW	1kW	50 [29]
Sub	Super	-	-	60 [30]
sub	Sub	-	-	60 [30]

6. Conclusion

Commercialisation of standalone DFIG will be a great leapfrogging in the development of microgrids especially in hybrid ones. Dynamic frequency tracking, that is devised, tested and presented by the authors in this paper, is new among the various techniques published in literature to regulate voltage and frequency in wind driven DFIG in standalone mode. DFT is much simpler than most of those and its implementation demands less number of components and fewer lines of coding too, staking ease in control and cool in maintenance. The testing carried out has been more or less comprehensive at this level of technology readiness. It included the two modes of generation – super synchronous and sub synchronous – and the system was tested under both steady state and transient conditions. Testing in steady state for different wind speeds demonstrated satisfactory operation in the two modes. Transient performance tests included load change as well as wind speed change, in both inter mode and intra mode transition of generation. The transient response of the DFT controlled standalone DFIG displayed fast transition during load change, wind power variation and mode change ensuring stability and reliability of the generation system on load.

The WT emulator used for the tests is carefully designed and validated. That the dynamic characteristics of the emulator is more challenging than that of a wind turbine on site – the WT emulator can yield faster wind speed changes and faster WT response – made the testing possible for conditions more vulnerable than those of the real field.

References

[1] J. Hamilton, M. Negnevitsky, X. Wang, and S. Lyden, "High penetration renewable generation within Australian isolated and remote power systems," *Energy*, vol. 168. pp. 684–692, 2019, doi: 10.1016/j.energy.2018.11.118.

[2] N. Bayati, H. R. Baghaee, A. Hajizadeh, and M. Soltani, "A Fuse Saving Scheme for DC Microgrids With High Penetration of Renewable Energy Resources," *IEEE Access*, vol. 8. pp. 137407–137417, 2020, doi: 10.1109/access.2020.3012195.

[3] O. Ogunrinde, E. Shittu, M. Bello, and I. E. Davidson, "Exploring the Demand-Supply Gap of Electricity in Nigeria: Locational Evaluation for Capacity Expansions," *2019 IEEE PES/IAS PowerAfrica*. 2019, doi: 10.1109/powerafrica.2019.8928645.

[4] M. L. de M. Galvão, M. L. de Medeiros Galvão, M. A. dos Santos, N. F. da Silva, and V. P. da Silva, "Connections Between Wind Energy, Poverty and Social Sustainability in Brazil's Semiarid," *Sustainability*, vol. 12, no. 3. p. 864, 2020, doi: 10.3390/su12030864.

[5] International Energy Agency, *World Energy Outlook 2019*. November 2019.

[6] S. Ghazi, "The Role of Decentralized Energy for Widening Rural Energy Access in Developing Countries," *Renewable Energy in the Service of Mankind Vol II*. pp. 291–299, 2016, doi: 10.1007/978-3-319-18215-5_26.

[7] A. Goswami, P. Sadhu, and P. K. Sadhu, "Development of a Grid Connected Solar-Wind Hybrid System With Reduction in Levelized Tariff for a Remote Island in India," *Journal of Solar Energy Engineering*, vol. 142, no. 4. 2020, doi: 10.1115/1.4046147.

[8] Y. Ikeda, "Power grid with 100% renewable energy for small island developing states," *Evolutionary and Institutional Economics Review*, vol. 17, no. 1. pp. 183–195, 2020, doi: 10.1007/s40844-019-00130-8.

[9] N. Bayati, H. R. Baghaee, A. Hajizadeh, and M. Soltani, "Localized Protection of Radial DC Microgrids With High Penetration of Constant Power Loads," *IEEE Systems Journal*. pp. 1–12, 2020, doi: 10.1109/jsyst.2020.2998059.

[10] A. Sanal, V. Mohan, M. R. Sindhu, and S. K. Kottayil, "Real time energy management and bus voltagedroop control in solar powered standalone DC microgrid," *2017 IEEE Region 10 Symposium (TENSYMP)*. 2017, doi: 10.1109/tenconspring.2017.8070056.

[11] S. Goel and R. Sharma, "Performance evaluation of stand alone, grid connected and hybrid renewable energy systems for rural application: A comparative review," *Renewable and Sustainable Energy Reviews*, vol. 78. pp. 1378–1389, 2017, doi: 10.1016/j.rser.2017.05.200.

[12] Aghaee, Aghaee, M. Dehkordi, Bayati, and Hajizadeh, "Distributed Control Methods and Impact of Communication Failure in AC Microgrids: A

Comparative Review," *Electronics*, vol. 8, no. 11. p. 1265, 2019, doi: 10.3390/electronics8111265.

[13] R. Pena, J. C. Clare, and G. M. Asher, "A doubly fed induction generator using back-to-back PWM converters supplying an isolated load from a variable speed wind turbine," *IEE Proceedings - Electric Power Applications*, vol. 143, no. 5. p. 380, 1996, doi: 10.1049/ip-epa:19960454.

[14] I. Boldea, "Variable Speed Generators." 2005, doi: 10.1201/9781420037265.

[15] S. N. Bhadra, D. Kastha, S. Banerjee, and S. Banerjee, *WIND ELECTRICAL SYSTEMS*. Oxford University Press, November 2005.

[16] A. K. Jain and V. T. Ranganathan, "Wound Rotor Induction Generator With Sensorless Control and Integrated Active Filter for Feeding Nonlinear Loads in a Stand-Alone Grid," *IEEE Transactions on Industrial Electronics*, vol. 55, no. 1. pp. 218–228, 2008, doi: 10.1109/tie.2007.911196.

[17] R. Resmi, V. Vanitha, T. N. P. Nambiar, and S. K. Kottayil, "Design and implementation of brushless doubly fed induction machine with new stator winding configuration," *Wind Engineering*. p. 0309524X1986842, 2019, doi: 10.1177/0309524x19868423.

[18] Y. Bakou and Saihi L, Hammaoui Y, Harrouz A, Colak I, Kayisli K, Abid M, Bayindir R. , "Robust Controller Based on Sliding Mode Technique of DFIG Integrated to Wind Energy System," 2019 7th *International Conference on Smart Grid (icSmartGrid)*. 2019, doi: 10.1109/icsmartgrid48354.2019.8990687.

[19] Allouche M, Abderrahim S, Zina HB and Chaabane M , "A Novel fuzzy Control Strategy for Maximum Power Point Tracking of Wind Energy Conversion System," *International Journal of Smart Grid*, vol.3, no.3, pp.120-7, September 2019.

[20] O. Anaya-Lara, N. Jenkins, J. B. Ekanayake, P. Cartwright, and M. Hughes, Wind Energy Generation: Modelling and Control. John Wiley & Sons, August 2011.

[21] A. Harrouz, I. Colak, and K. Kayisli, "Energy Modeling Output of Wind System based on Wind Speed," 2019 8th International Conference on Renewable Energy Research and Applications (ICRERA). 2019, doi: 10.1109/icrera47325.2019.8996525.

[22] G. Abad, J. Lopez, M. Rodriguez, L. Marroyo, and G. Iwanski, Doubly Fed Induction Machine: Modeling and Control for Wind Energy Generation. John Wiley & Sons, September 2011.

[23] L. Guo, D. Wang, Z. Peng, and L. Diao, "Improved super-twisting sliding mode control of a stand-alone DFIG-DC system with harmonic current suppression," *IET Power Electronics*, vol. 13, no. 7. pp. 1311–1320, 2020, doi: 10.1049/iet-pel.2019.0691.

[24] M. R. and S. T. K. C., "Detailed modelling and development of a laboratory prototype for the analysis of subsynchronous resonance in DFIG-based wind farm," International Transactions on Electrical Energy Systems, vol. 30, no. 3. 2020, doi: 10.1002/2050-7038.12245.

[25] I. Erazo-Damian, J. M. Apsley, R. Perini, M. F. Iacchetti, and G. D. Marques, "Stand-Alone DFIG FOC Sensitivity and Stability Under Mismatched Inductances," IEEE Transactions on Energy Conversion, vol. 34, no. 2. pp. 860–869, 2019, doi: 10.1109/tec.2018.2869286.

[26] L. Guo, D. Wang, Z. Peng, and L. Diao, "Direct voltage regulation of a stand-alone DFIG system with non-linear loads based on an improved-extended state observer and SSM control," IET Renewable Power Generation, vol. 13, no. 11. pp. 1891–1901, 2019, doi: 10.1049/iet-rpg.2018.6045.

[27] "Power Converters in Wind Energy Conversion Systems," Power Conversion and Control of Wind Energy Systems. pp. 87–152, 2011, doi: 10.1002/9781118029008.ch4.

[28] M. Quraan, Q. Farhat, and M. Bornat, "A new control scheme of back-to-back converter for wind energy technology," 2017 IEEE 6th International Conference on Renewable Energy Research and Applications (ICRERA). 2017, doi: 10.1109/icrera.2017.8191085.

[29] E. Elbouchikhi, G. Feld, Y. Amirat, M. Benbouzid, and F. Le Gall, "Design and experimental implementation of a wind energy conversion platform with education and research capabilities," Computers & Electrical Engineering, vol. 85. p. 106661, 2020, doi: 10.1016/j.compeleceng.2020.106661.

[30] K. Ji, W. Long, and J. He, "Indirect Vector Control for Stand-alone Operation Brushless Doubly Fed Induction Generator Employing Power Winding Stator Flux Orientated Approach," IOP Conference Series: Materials Science and Engineering, vol. 612. p. 042085, 2019, doi: 10.1088/1757-899x/612/4/042085.

[31] A. Vijayakumari, A. T. Devarajan, and N. Devarajan, "Decoupled control of grid connected inverter with dynamic online grid impedance measurements for micro grid applications," International Journal of Electrical Power & Energy Systems, vol. 68. pp. 1–14, 2015, doi: 10.1016/j.ijepes.2014.12.015.

[32] K. Vijayakumar, N. Kumaresan, and N. G. A. Gounden, "Operation of inverter-assisted wind-driven slip-ring induction generator for stand-alone power supplies," IET Electric Power Applications, vol. 7, no. 4. pp. 256–269, 2013, doi: 10.1049/iet-epa.2012.0139.

[33] K. Vijayakumar, S. B. Tennakoon, N. Kumaresan, and N. G. A. Gounden, "Real and reactive power control of hybrid excited wind-driven grid-connected doubly fed induction generators," IET Power Electronics, vol. 6, no. 6. pp. 1197–1208, 2013, doi: 10.1049/iet-pel.2012.0709.

[34] Mishra V, Shukla RD and Gupta P, "An approach towards Application of Semiconductor Electronics Converter in Autonomous DFIM based Wind Energy Generation System: A Review," International Journal

of Smart Grid, vol.3, no.3, pp.152-62, September 2019.

[35] Soued, S., Chabani, M.S., Becherif, M., Benchouia, M.T., Ramadan, H.S., Betka, A., Golea, A. and Zouzou, S.E., "Experimental behaviour analysis for optimally controlled standalone DFIG system," *IET Electric Power Applications*, vol. 13, no. 10. pp. 1462–1473, 2019, doi: 10.1049/iet-epa.2018.5648.

[36] I. Attoui and A. Omeiri, "Modeling, control and fault diagnosis of an isolated wind energy conversion system with a self-excited induction generator subject to electrical faults," *Energy Convers. Manage.*, vol. 82, pp. 11–26, June 2014, doi: 10.1016/j.enconman.2014.02.068.

[37] B. Touaiti, H. B. Azza, and M. Jemli, "Control Scheme for Stand-alone DFIG Feeding an Isolated Load," *2019 10th International Renewable Energy Congress (IREC)*. 2019, doi: 10.1109/irec.2019.8754515.

[38] F. Martinez, L. Carlos Herrero, and S. de Pablo, "Open loop wind turbine emulator," *Renewable Energy*, vol. 63. pp. 212–221, 2014, doi: 10.1016/j.renene.2013.09.019.

[39] Nouira I, Khedher A and Bouallegue A, "A Contribution to the Design and the Installation of an Universal Platform of a Wind Emulator using a DC Motor," *International Journal of Renewable Energy Research,* vol.2, no.2, pp. 797-804, December 2012.

[40] S. Heier, *Grid Integration of Wind Energy: Onshore and Offshore Conversion Systems*. John Wiley & Sons, April 2014.